

Compression Behaviors of Wood-based Lattice Sandwich Structures

Dongxia Yang,^{a,b,*} Yingcheng Hu,^b and Changsheng Fan^b

To obtain a lightweight and high-strength wood sandwich structure, a wooden lattice sandwich cell element was designed in combination with a pyramid-type structure. After inserting glue to prepare the cell unit, the influence of panel thickness and core diameter on the unit cell force was analyzed and compared under the condition of flat pressure. Under the condition of flat pressure, the specific strength of the unit cell was higher than that of the specific strength of the composition material, and the unit cell may be regarded as a structure with high specific strength. Theoretical predictions, simulation analysis, and experimental tests demonstrated that the structure compressive capacity depended on the diameter of the core when the core length was set. The larger the diameter of the core is, the stronger the bearing capacity of the unit cell will be. When the diameter of the core is constant, the longer the core length is, the weaker the bearing capacity of the unit cell will be. The simulation analysis was in agreement with the experimental test results, indicating that the destruction of the structure was mainly caused by the failure of the core.

Keywords: Wood engineering material; Lattice structure; Sandwich structure; Plane pressure characteristics

Contact information: a: Harbin University Key Laboratory of Heilongjiang underground engineering technology, Harbin University, Harbin 150086, China; b: Key Laboratory of Bio-based Material Science and Technology of Ministry of Education of China, College of Material Science and Engineering, Northeast Forestry University, Harbin 150040, China;

* Corresponding author: gongxydx@hrbu.edu.cn

INTRODUCTION

In the last few decades, the sandwich structure has been rapidly and extensively developed in various materials (Wu and Pan 2009), and the lattice structure has been inspired by ultra-light porous material found in nature (Schaedler *et al.* 2011). Researchers have been studying lightweight materials with a lattice structure ever since the space lattice material was proposed (Ashby 2001; Evans *et al.* 2001; Gibson *et al.* 2010). The main lattice structures are pyramidal (Xiong *et al.* 2011; Mu *et al.* 2016; Chen *et al.* 2017), tetrahedral (Wadley *et al.* 2003; Zhao *et al.* 2016; Shi *et al.* 2017), woven hollow fibers (Fan *et al.* 2007b; Wu *et al.* 2012), and Kagome (Wang *et al.* 2003; Hwang *et al.* 2016). Most of these structures are made of metal and other composite materials. Research has been carried out with biomass materials, such as balsa wood (Bekisli and Grenestedt 2004), cork (Kral *et al.* 2014), paper based corrugated structures (Hunt *et al.* 2004), plywood as a corrugated core material for sandwich panels (Bhattacharyya *et al.* 2011), wood based two dimensional lattice truss core sandwich structures (Jin *et al.* 2015), natural fiber based isogrid lattice cylinder (Hao *et al.* 2017), and sandwich panel with interlocking plywood kagome lattice core (Klimek *et al.* 2016).

Biomass materials, such as wood, bamboo, hemp, *etc.*, play a critical role in human production and life as structural materials. Wood is a type of natural, renewable, and recyclable material with a high strength-to-weight ratio, as well as high thermal and sound insulation performance (Lata *et al.* 2016; Zhu and Luo 2017). To meet the requirements of modern wood construction, the lattice structure is often applied to wood engineering materials, as it is considered a structure with enormous development potential (Han and Tsai 2003; Fan and Yang 2007a). This structure conforms to the developmental trends in wood-based engineering materials of materials that integrate form and function, are both lightweight and high-strength, and are environmentally friendly.

This study used 3D printing technology to create the sandwich structure proposed by some contemporary scholars (Li and Wand 2017). The flat pressure test was conducted, and the best structure was applied to the wood engineering material. The unit sandwich structure was designed to adhere to the characteristics of wood-based engineering materials and lattice structures. Theoretical prediction, simulation analysis, and experimental results were performed in an out-of-plane compressive experiment. The influencing factors were analyzed for their diverse strength-to-weight ratios, and the differences between the theoretical prediction, simulation analysis, and experimental results were investigated.

SIMULATION

Unit Cell Structure Optimization

Most of the existing research on the sandwich structure is about the configuration and preparation process of metal and composite materials. The most common sandwich structure types are tetrahedron, pyramid, triangular prism, rectangular pyramid, dodecahedron, *etc.* Tetrahedron, pyramid, and pyramid-like (where the angle between the core and bilateral panels is 45°) structures have been widely studied. The tetrahedron is the simplest regular polyhedron, where the angle between the core and the bilateral panels is 54.8° , and the pyramid has the most stable angle, so the angle between the core and the bilateral panels is 52° . Most researchers only explore one of the types to analyze the mechanics and do not compare the different sandwich structures. In this study, these three types of unit structures were printed using 3D printing technology. All of the printed structures consisted of the same material, had the same thickness for the bilateral panels, and the same core diameter. Polylactic acid (PLA) material was elected as the 3D printing material to make sure that the unit structure model was of isotropic homogenization. The stress state and failure form of the unit structure were observed, as shown in Fig. 1.

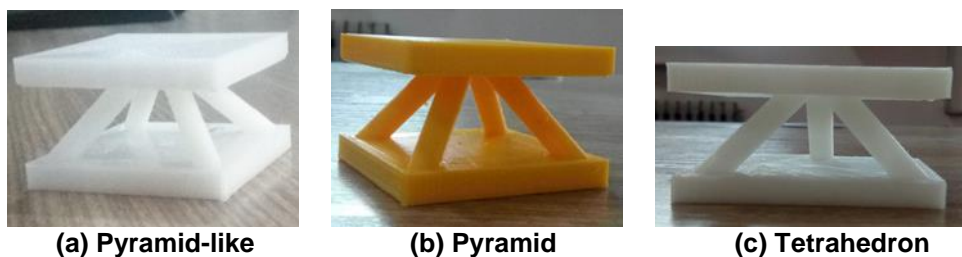


Fig. 1. Models of the three types of unit structures

As a result of the different structures, there were some differences in height. The size of each model is expressed in terms of length (mm) \times width (mm) \times height (mm). The sizes of the models shown in Fig. 1 were as follows: (a) 43 mm \times 43 mm \times 26 mm, (b) 43 mm \times 43 mm \times 28 mm, and (c) 43 mm \times 43 mm \times 28 mm. The dimensions of the panels were 43 mm \times 43 mm \times 10 mm, and the diameter of each core was 10 mm. A universal mechanical testing machine (WDW-300, Changchun Kexin Test Instrument Co., Ltd., Changchun, China) was utilized to conduct the out-of-plane compressive experiment with 5 specimens in the same structure.

Simulation Results

The compressive load and displacement curves are shown in Fig. 2.

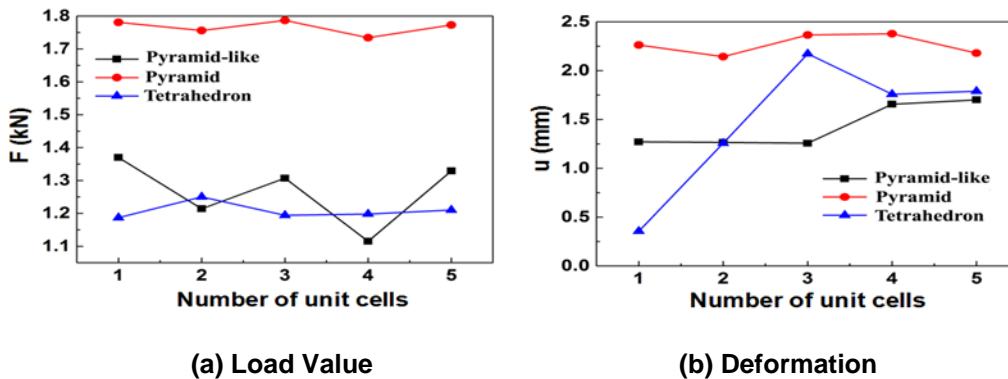


Fig. 2. Contrast diagram of different unit structures' load and displacement

The pyramid unit structure had the strongest compressive capacity (Fig. 2(a)). The fluctuation of the pyramid-like unit was more intense, but its average value was still higher than that of the tetrahedron unit. The pyramid unit structure had the largest deformation (Fig. 2(b)). The fluctuation of the pyramid-like unit was still intense, and its average value was still higher than that of the tetrahedron. As the load increased, the failure mode of the pyramid-like structure was brittle fracture of the sandwich core. The failure mode of the tetrahedron structure was the initial creep crushing of the sandwich core, and consequential brittle fracture of the core. The core of the pyramidal structure failed by creep crushing until the up-panel and down-panel were integrated with the core, which demonstrated great energy absorption. Fluctuations in the load and displacement diagrams of the tetrahedron and pyramid-like structures were due to the brittle fracture of the core in both structures.

Unit Cell Structure

Based on the results, the pyramid unit had the best compressive behaviors of the three structures; its lattice matrix sandwich cell structure is shown in Fig. 3.

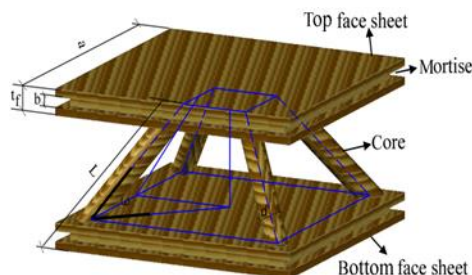


Fig. 3. Schematic of wood-based lattice sandwich unit cell structure

This cell structure was made up of a top face sheet, a bottom face sheet, and cores in between the sheets. The angle between the panel and each core was 52° . The bilateral panels of the unit cell were square-shaped, the width of which was a mm, the thickness t_f mm, the mortise depth b mm, the diameter of each core d mm, and the length l mm. Through the insertion of the mortise and tenon in the tenon and grooves between the cell elements, structural forms such as a network frame, hollow plate, beam, column, *etc.*, could be created. Additionally, the cell size could be changed, being dependent on the application requirements to enlarge the application range. This method ties in with the current rigorous development of assembled wooden structures (GB/T 51233 2016; Liu and Cao 2017).

Analysis

Mechanical property analysis

The mechanical strength of the lattice sandwich unit cell depends on the strength of the panel, the strength of the core, and the bonding strength between them, which jointly determines the bearing capacity of the structure. Because the preparation process of the lattice structure was still immature in terms of development, the main mechanical property focused on what was the flat compressive performance of the cell.

Uniform flat-load, out-of-plane stress was applied on the structure in Fig. 3, and its stress was analyzed. The connection between the cores and panels was an effectively permanent connection. These four cores bore the most stress under the load state, and the vertical load of each core was expressed as F . The force diagram of the core is shown in Fig. 4.

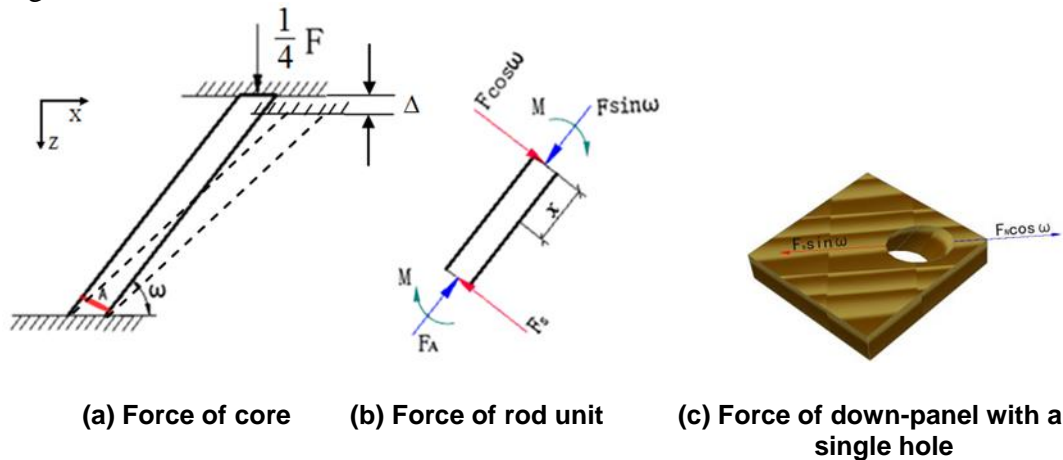


Fig. 4. Force analysis

The geometric relations concluded through Fig. 4 are as follows,

$$\text{Axial force: } F_A = F \sin \omega \quad (1)$$

$$F_A = ES \frac{\Delta l}{l} = E\pi \left(\frac{d}{2}\right)^2 \frac{\Delta \cdot \sin \omega}{l} \quad (2)$$

In Eq. 2, d is the diameter of core elements (mm), l is the length of the core (mm), Δ is deformation of the unit cell (mm), and E is elastic modulus of core material (MPa).

$$\text{Shear force: } F_s = F \cos \omega \quad (3)$$

$$\text{Bending moment: } M = F \cos \omega \cdot x \quad (4)$$

In Eqs. 3 and 4, x is the distance (mm) between the shear force and the stress point ($0 \leq x \leq l$) (mm), l is the length of the core (mm), and ω is the angle between the core and the panel (angle),

$$\text{Stress on the hole of panel: } \sigma = \frac{F_s \sin \omega + F_A \cos \omega}{\pi d t_f} \quad (5)$$

where d is the diameter of core (mm), and t_f is the thickness of panel (mm).

$$\text{Axial stress: } \sigma_1 = \frac{F_A}{s} = \frac{F \sin \omega}{\pi \left(\frac{d}{2}\right)^2} \quad (6)$$

$$\text{Maximum shear stress: } \tau_{\max} = \frac{4 F_s}{3 s} = \frac{4}{3} \frac{F_s}{\pi \left(\frac{d}{2}\right)^2} \quad (7)$$

$$\text{Bending stress: } \sigma_{II} = \frac{M}{\pi d^3 / 64} \quad (8)$$

The stress of the rod unit was the sum of axial stress, maximum shear stress, and bending stress under the force F . According to the stress state of the rod unit, it can be concluded that the stress on the upper surface was the difference between the bending stress and the axial stress, while the stress on the lower surface was the sum of the bending stress and the axial stress. The neutral bearing of the rod unit was subjected to the maximum shear stress, τ_{\max} . Therefore, the position of danger on the rod unit can be seen in Fig. 4(a), at point A and the position below the centerline of the rod unit near A.

Figure 4(c) shows in the stress analysis of the single-hole lower panel. According to equation (4), it can be seen that the stress decreased with increasing thickness of the panel under the combined force of the shear force acting on the panel $F_s \sin \omega$ and the axial force acting on the panel of $F_A \cos \omega$. This result indicated that a thinner panel resulted in a greater amount of stress on the panel. Under the force, the lower panel split along the texture direction near the hole, and the upper panel split in the same way.

The relationship between the compressive capacity of the core and its length and diameter under the material's ultimate stress state is shown in Fig. 5. In the ultimate stress state of the material, according to Eq. 2, the relationship between the core bearing capacity and its length and diameter is shown in Fig. 5.

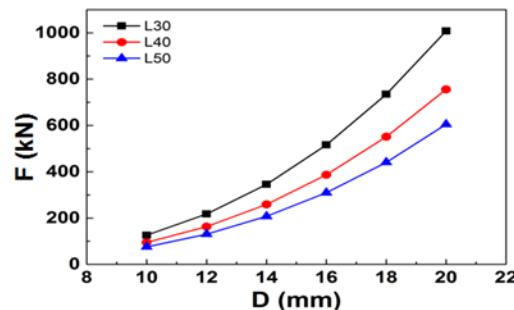


Fig. 5. Length, diameter, and axial force of the cores

The notations L30 to L50 in the figure indicate that the core length was 30 mm to 50 mm, from which it can be concluded that the length and diameter of the core have a non-linear relationship with its force. When the radius increased, the increasing trend of

cores with various lengths was the same. When the core length was fixed, as the core diameter increased, so did the compressive capacity. When the core diameter was attached, as the core length increased, compressive capacity decreased, which indicated that longer cores bore smaller shear force and bending moment.

Modeling analysis

The unit cell was primarily composed of bilateral panels and cores. Three cell structures were defined according to the relationship between the panel thickness and core diameter: when the panel thickness was less than the core diameter it was defined as model A; when the panel thickness was larger than the core diameter it was defined as model B; and when the panel thickness was equal to the core diameter it was defined as model C. The stress states and deformation of these three structures were analyzed using ANSYS simulation (ANSYS 15.0, Ansys, Canonsburg, PA, USA). The simulation conditions were set as such: the down-panel was horizontally fixed, a uniform load was implemented at the up-panel, the panel material was larch, and the core material was birch. The three structures were modeled and analyzed on this basis. The simulation parameters are given in Table 1.

Table 1. Simulation parameters of unit cell structure (mm)

Thickness of Panel, t_f	Diameter of Core, d		
	Specimen A	Specimen B	Specimen C
12	16	10	12

The out-of-plane compressive simulated stress for the three types of models is shown in Fig. 6. The maximum stress in every type of model occurred on the core, and was mostly near the root of the core, which was consistent with the theoretical analysis.

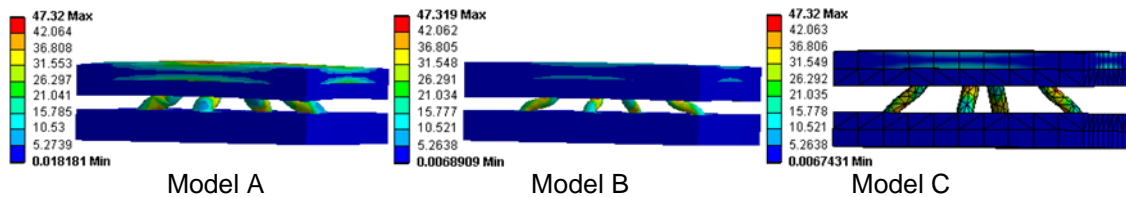


Fig. 6. Stress of three unit cell models

The compressive strength of the birch core was 47.3 MPa (Jiang *et al.* 2010), and the maximum stress value in Fig. 6 was the ultimate compressive value of the core. The load and deformation under stress for the three unit cells are compared in Fig. 7.

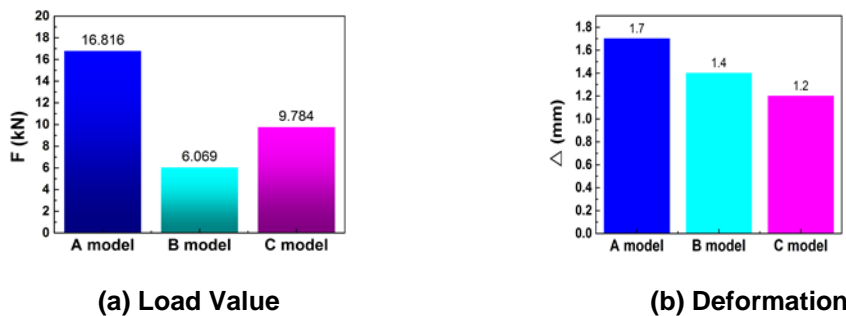


Fig. 7. Comparison of the compression state of the three unit cell models

The maximum load was observed in the model A cell unit, at 16.8 kN. The smallest load was observed in the model B unit cell at 6.07 kN, and the load of the model C unit cell was intermediate to the other two models at 9.78 kN. The model that attained maximum deformation was the model A unit cell, with 1.70 mm deformed. The model with the smallest deformation was the model C unit cell, with 1.20 mm deformed, and the model B unit cell was again intermediate to the other two models at 1.40 mm.

EXPERIMENTAL PROGRAM

Materials

Northeastern larch was purchased from Comprehensive processing factory Yichun Dailing Wood Products, Yichun, China. The mechanical properties of northeastern larch were described previously (Jiang *et al.* 2010): the density is 0.61g/cm³, compressive strength parallel to grain from 44.2MPa to 56.49MPa, the modulus of elasticity by static bending test from 9.51GPa to 15.51GPa. The ultimate strain under elastic deformation from 0.0058 to 0.0090 μm (Zhou *et al.* 2016).

Birch was purchased from Jiqing Wood Products, Linyi, China. The mechanical properties of birch were described previously (Jiang 2015; Jiang *et al.* 2017): the density is 0.59 g/cm³, compressive strength parallel to grain is 47.32 MPa, and the modulus of elasticity by static bending test from 7.7G Pa to 9.3G Pa. The ultimate strain under elastic deformation is from 0.05 to 0.012 μm (Wang *et al.* 2012). The adhesive used, modified epoxy resin (J-22B/C), was obtained from Institute of Petrochemistry Heilongjiang Academy of Sciences, Harbin, China.

Material Properties and Fabrication

The panel size was 2440 mm \times 1220 mm \times 12 mm, and the panel was whole larch finger-jointing board. A circular saw machine was used to cut sample panels to size 185 mm \times 185 mm \times 12 mm. Three kinds of cell models were selected: A, B, and C with matching dimensions of 10 mm, 16 mm, and 12 mm. Holes were drilled at an angle of 52° in the panel, according to the designed unit cell structure. Moderate adhesive was applied into the drilling holes, and then the dowels were inserted and assembled with the up-panel and down-panel, adjusting the distance between the bilateral panels. The prepared specimens were set for 72 h. After 72 h, the planing saw was used to keep the specimen at an absolute level. The specimen preparation was then complete, and the specimen was ready for testing. Three models of the unit cell structures are shown in Fig. 8, of which model C was designed according to the Fig. 2 cell structure.

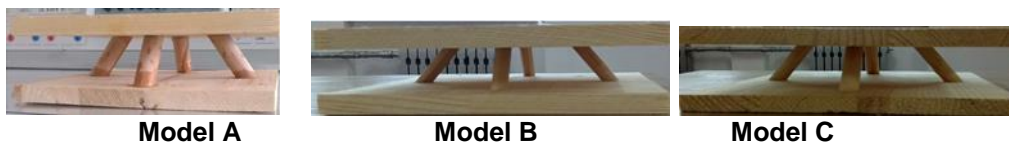


Fig. 8. Wood models of the three unit cell structures

Performance Testing

The tests were carried out in accordance with the GB/T 1453 (2005) standard. A universal mechanical testing machine (Changchun Kexin Test Instrument Co., Ltd.,

Changchun, China) was used to test the vertical compressive behaviors of these three sandwich structure samples at a rate of 2 mm/min. The test is shown in Fig. 9.

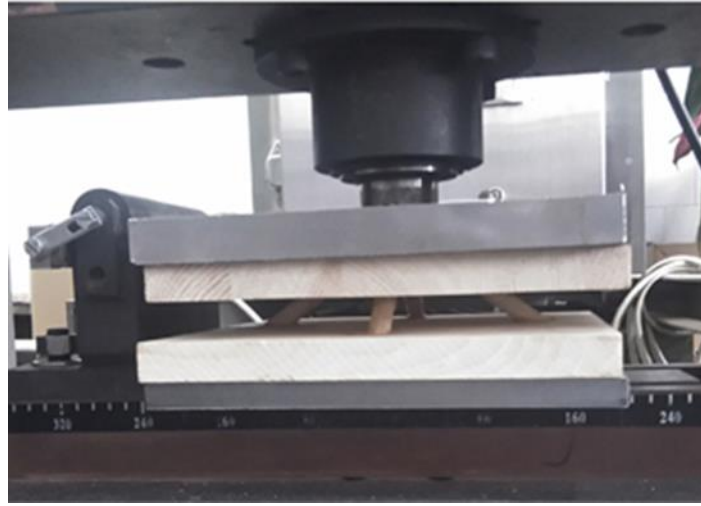


Fig. 9. Out-of-plane flat compression test of sandwich structure

RESULTS

Loading and Response

The three cell test curves are given in Fig. 10. It can be observed in the curve that the A-cell had the largest bearing capacity, with a value of 18.9 kN, and the B-cell capacity was the smallest with a value of 11.9 kN. The C-cell capacity was between the two, at 14.4 kN. B-cells exhibited the best linearity, but they are also given the lowest energy absorption.

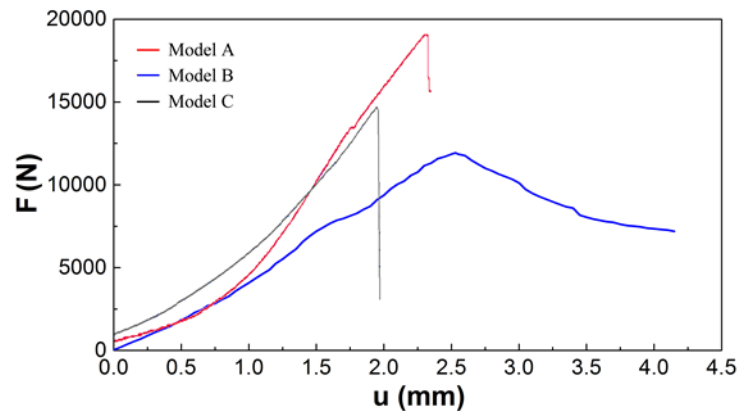


Fig. 10. Load-displacement curve of the three unit cell models

In order to compare and analyze the compression properties of three unit cell structures, the specific strengths of the three cell structures were calculated. The calculated results are shown in Table 2.

As be obtained from Table 2, Model B had the highest specific strength, model A had the lowest specific strength, and the specific strength of model C was intermediate

between those of the previous two models. However, the specific strengths of the three cell models were all higher than the models made of one single wood material.

Table 2. Properties of the Unit Cells Under Stress

Name	Maximum Load, F (kN)	Limit Stress, σ (MPa)	Relative Density, ρ (kg/m ³)	Quality, m (kg)	Specific Strength, σ/ρ (10 ³ Nm/kg)
Model A	18.89	23.64	247.23	0.440	95.62
Model B	11.93	35.03	240.49	0.428	145.67
Model C	14.45	32.07	241.61	0.430	132.73
Larch	—	44.2	610	—	72.46
Birch	—	47.32	590	—	80.20

The destruction of the test models under the ultimate load is shown in Fig. 11. In model A, cracks emerged in the cell panel. The right side had cracks through the board from the top to the bottom, while the left side had cracks through half of it, and the dowels were intact. In model B, the panel was intact, but the up-and-down-panels became twisted, and the dowels underwent both bending deformation and fracture failure. In model C, the bilateral panels cracked, with the down-panel sustaining greater damage, and the dowels were also broken, primarily near the roots.



Destruction of model A

Destruction of model B

Destruction of model C

Fig. 11. Destruction of the unit cell structures

Comparing the three factors of cell bearing capacity, specific strength, and quality, the overall performance of C-type unit cells was better than that of A-type and B-type. In order to determine the effect of core length on unit cell stress, the length of the c-type unit cell core was changed, as is shown in Fig. 12. In the figure, when core length L was 54 mm, the cell carrying capacity was 12.5 kN; when L was 56 mm, the cell bearing capacity was 10.4 kN; when L was 58 mm, the cell bearing capacity was 8.94 kN. In Fig.10, when the core length L was 52 mm, the bearing capacity of the unit cell was 14.4 kN. It can be concluded that the longer the core size is, the weaker the bearing capacity of the cell will be. This conclusion is in accordance with the theoretical results shown in Figure 5.

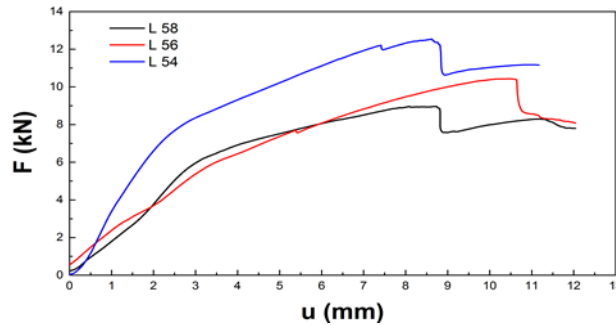


Fig. 12. The force curve of C type unit cell with different length of cores

DISCUSSION

Through theoretical prediction, simulation, and experiment, the compression ability of the unit cell structure was analyzed. It can be concluded that the bearing capacity of the unit cell is proportional to the diameter of the core under the action of a flat pressure load, and is inversely proportional to the length of the core. That is, the larger the diameter of the core is, the stronger the bearing capacity of the unit cell will be. The longer the core length is, the weaker the bearing capacity of the unit cell will be. The specific strength of the unit cell is inversely proportional to the diameter of the core; that is, the larger the diameter of the core is, the lower the specific strength of the unit cell will be. The specific strength is an important index to measure the light-weight and high-strength of materials. The greater the strength is, the better the lightweight and high-strength material will be. Therefore, under the condition of flat pressure, the main body of the unit cell is cores. However, the larger the diameter of the core is, the worse will be the performance of the unit cell. The specific strength of the three unit cell structures is higher than the specific strength of the single species. Therefore, the pyramid-type wooden grid structure is a structure having a higher specific strength in natural biomass materials.

Through the analysis of three kinds of pyramidal unit cell, it can be concluded that the unit cell type with the same thickness and core diameter has the smallest deformation. For wood materials, the larger the core diameter size, the larger the pore size on the processed panel. From the comprehensive comparison of the two factors of unit cell bearing capacity and deformation, the overall performance of C unit cell is better than that of A and B unit cells. In the simulation analysis, the ultimate stress value of the core material is used to determine whether the cell element is damaged or not, and the bearing capacity of the plastic deformation of the panel, adhesive and material in the compression process is not considered, because it is difficult to simulate these quantities in the simulation analysis.

A comparison of unit cell destruction is shown in Table 3. According to the theoretical calculations, the destruction of the core appeared near the root, and the stress exerted on the panel was not enough to break the panel. Simulation analysis can also be used to predict the destruction of the three types of unit cells, making sure that the destruction is consistent with the experimental results.

Table 3. Comparison of Cell Destruction

Name	Model A	Model B	Model C
Theoretical Prediction	Panel is damaged	Core is damaged	Both panel and core are damaged
Simulation Results	Panel deformation is maximum	Core bears the maximum stress	Panel deformation is greater than the cores'
Experimental Results	The root of the core (the junction of panel and core) was broken		

Simulation analysis and experimental results showed that with increasing core diameter, the compressive capacity of the unit cell was enhanced and the deformation of the panel became more severe. Increasing the thickness of the panel reduced the degree of damage to the panels. However, the quality of the unit cell was also increased. Therefore, future work will focus on finding a balance between thick panels, large core diameter, and the characteristics of low weight and high strength.

CONCLUSIONS

This study aimed to investigate a natural biomass material structure, which was advantageous in its low weight and high strength. The results indicated that the wood-based two-dimensional lattice sandwich structure had a higher specific strength than the material itself. In this study, three types of unit cell structures—tetrahedron, pyramid-like, and pyramid—were printed using 3D printing technology. The out-of-plane compressive behaviors of the sandwich structures were examined using experimental methods, in which the pyramid structure had the best compressive performance. Dividing the pyramidal unit cell into three different types, and through some theoretical calculations, simulation analysis, and experimental results, the following was concluded:

1. The specific strength of the wood-based lattice sandwich structures was higher than the strength of the material itself, which was in accordance with the characteristics of the natural material structure of light quality and high strength.
2. Under the ultimate load, the compressive capacity of the unit cell was closely related to the core length and diameter. When the length of the core was fixed, the compressive capacity increased as the diameter of the core increased.
3. Under the ultimate stress state of the component, the diameter of the core was directly proportional to the carrying capacity of the unit cell, which was inversely proportional to the specific strength of the unit cell. Thus, a larger core diameter resulted in a stronger cell flat-pressing ability, but the performance was not optimal.
4. Based on the analysis of the cell structure, one can connect the triplets of C-cells, as shown in Fig. 13.



Fig. 13. Connection of three unit cells

Continuing the approach shown in Fig. 13, one can also connect more unit cells to form space plates, beams and columns, and become a wooden sandwich structure with large design space and light weight and high strength. Through this form, the integration of structural design, preparation, characterization, evaluation and application of wood engineering materials can be realized. Therefore, in the future cellular structure design, the flat pressure carrying capacity of the unit cell structure can be improved by changing the unit cell material or integrating the unit cells.

ACKNOWLEDGMENTS

The support of the Doctoral Foundation of Harbin University (HUDF2014), Postdoctoral Science Foundation of China (2017M611339), Science Planning Project of Education in Heilongjiang Province (GBB1317063), and National Natural Science Foundation of China (31470581) are gratefully acknowledged.

REFERENCES CITED

- Ashby, M. F. (2001). "Drivers for material development in the 21st century," *Progress in Materials Sciences* 46(3-4), 191-199. DOI: 10.1016/S0079-6425(00)00014-1
- Bekisli, B., and Grenestedt, J. L. (2004). "Experimental evaluation of a balsa sandwich core with improved shear properties," *Composites Science and Technology* 64(5), 667-674. DOI:10.1016/S0266-3538(03)00294-X.
- Bhattacharyya, D., Kavermann, S., Penneru, P., and Rao, S. (2011). "Veneer based lightweight sandwich panel for high end interior applications: Manufacturing, evaluation and cost analysis," *Joint International Symposium on Wood Composites and Veneer Processing and Products*, Washington State University, Pullman, WA, pp.1-11.
- Chen, F., Jin, X., Zhang, Q., Yuan, X., Lu, X., and Zhu, X. (2017). "Numerical method for bending strength of composite lattice sandwich structure containing hole under external load," *Acta Materiae Compositae Sinica* 34(2), 1-11. DOI: 10.13801/j.cnki.fhclxb.20170222.007
- Evans, A. G., Hutchinson, J. W., Fleck, N. A., Ashby, M. F., and Wadley, H. N. G. (2001). "The topological design of multifunctional cellular metals," *Progress in Materials Science* 46(3-4), 309-327. DOI: 10.1016/S0079-6425(00)00016-5
- Fan, H., and Yang, W. (2007a). "Development of lattice materials with high specific stiffness and strength," *Advances in Mechanics* 37(1), 99-112.
- Fan, H., Yang, W., Fang, D., Zhuang, Z., Chen, X., Xing, L., Li, B., and Jiang, S. (2007b). "Interlacing technique for new carbon fiber lattice materials," *Journal of Aeronautical Materials* 27(1), 46-50.

- GB/T 1453-2005 (2005). "Test method for flatwise compression properties of sandwich constructions or cores," Standardization Administration of China, Beijing, China.
- GB/T 51233-2016 (2016). "Technical standard for prefabricated timber buildings," Standardization Administration of China, Beijing, China.
- Gibson, L. J., Ashby, M. F., and Harley, B. A. (2010). *Cellular Materials in Nature and Medicine*, Cambridge University Press, Cambridge, UK.
- Han, D. Y., and Tsai, S. W. (2003). "Interlocked composite grids design and manufacturing," *Journal of Composite Material* 37(4), 287-316. DOI: 10.1177/0021998303037004681
- Hao, M., Hu, Y., Wang, B., and Liu, S. (2017). "Mechanical behavior of natural fiber based isogrid lattice cylinder," *Composite Structures* 176, 117-123. DOI: 10.1016/j.compstruct.2017.05.028
- Hunt, J. F., Harper, D. P., and Friedrich, K. A. (2004). "Three dimensional engineered fiberboard: Opportunities for the use of low valued timber and recycled material," *38th International Wood Composites Symposium*, Washington State University, Pullman, WA, pp.207-2016.
- Hwang, J. S., Choi, T. G., Lee, D., Lyu, M. Y., Lee, D. G., and Yang, D. Y. (2016). "Development of a bendable pyramidal kagome structure and its structural characteristics," *Composite Structures* 142, 87-95. DOI: 10.1016/j.compstruct.2016.01.079
- Jiang, X., Cheng, Y., and Yin, Y. (2010). *Chinese Gymnosperms of Wood*, Science Press, Beijing, China.
- Jiang, Z. (2015). *Wood Properties of the Global Important Tree Species*, Science Press, Beijing, China.
- Jiang, J. H., Yu, Z. Z., and Zhao, L. Y. (2017). "Study on compression strength parallel to grain of birch wood at low temperature," *Journal of Forestry Engineering* 04(2), 30-33. DOI:10.13360/j.issn.2096-1359.2017.04.005
- Jin, M., Hu, Y., and Wang, B., and Sebera, V. (2015). "Compressive and bending behaviours of wood-based two-dimensional lattice truss core sandwich structures," *Composite Structures* 124, 337-344. DOI: 10.1016/j.compstruct.2015.01.033
- Klimek, P., Wimmer, R., Brabec, M., and Sebera, V. (2016). "Novel sandwich panel with interlocking plywood kagome lattice core and grooved particleboard facings," *BioResources* 11(1), 195-208. DOI: 10.15376/biores.11.1.195-208
- Kral, P., Klimek, P., Mishra, P. K., Rademacher, P., and Wimmer, R. (2014). "Preparation and characterization of cork layered composite plywood boards," *BioResources* 9(2), 1977-1985. DOI: 10.15376/biores.9.2.1977-1985.
- Lata, K., Dubey, B., and Misra, A. K. (2016). "Modeling the effects of wood and non wood based industries on forestry resources," *Natural Resource Modeling* 29(4), 559-580. DOI: 10.1111/nrm.12111
- Li, T., and Wang, L. (2017). "Bending behavior of sandwich composite structures with tunable 3D printed core materials," *Composite Structures* 175, 46-57. DOI: 10.1016/j.compstruct.2017.05.001
- Liu, J., and Cao, C. (2017). "Prefabricated timberwork system application in contemporary architectural design," *Standardization of Engineering Construction* (4), 18-19.
- Mu, J., Li, Y., Zhang, Z., and Peng, F. (2016). "Failure analysis of cell sandwich plate with pyramidal lattice cores under vertical impact," *Journal of Naval University of Engineering* 28(6), 5-9.

- Schaedler, T. A., Jacobsen, A. J., Torrents, A., Sorensen, A. E., Lian, J., Greer, J. R., Valdevit, L., and Carter, W. B. (2011). "Ultralight metallic microlattice," *Science* 334(6058), 962-965. DOI: 10.1126/science.1211649
- Shi, Y., Chen, J., Ge, W., Liu, J., and Wang, X. (2017). "Vibration characteristics of sandwich beam with pyramidal truss core," *Journal of Dynamics and Control* 15(4), 314-323.
- Wadley, H. N. G., Fleck, N. A., and Evans, A. G. (2003). "Fabrication and structural performance of periodic cellular metal sandwich structures," *Composites Science and Technology* 63(16), 2331-2343. DOI: 10.1016/S0266-3538(03)00266-5
- Wang, J., Evans, A. G., Dharmasena, K., and Wadley, H. N. G. (2003). "On the performance of truss panels with Kagome cores," *International Journal of Solids and Structures* 40(25), 6981-6988. DOI: 10.1016/S0020-7683(03)00349-4
- Wang, P., Chen L., Ji X., Song H., and Gou F. (2012). "Analysis of stress strain curves for four common arbor root systems," *Bulletin of Soil and Water Conservation* 32(3), 17-22.
- Wu, L., and Pan, S. (2009). "Survey of design and manufacturing of sandwich structures," *Materials China* 28(4), 40-45.
- Wu, L., Xiong, J., Ma, L., Wang, B., Zhang, G., and Yang, J. (2012). "Processes in the study on novel composite sandwich panels with lattice truss cores," *Advances in Mechanics* 42(1), 41-67.
- Xiong, J., Ma Li, Yang, J., and Wu, L. (2011). "Fabrication and mechanical response of carbon fiber sandwich panels with pyramidal truss cores," *Chinese Journal of Solid Mechanics* 32(10), 8-13.
- Zhao, B., Li, Z., Hou, H., Han, X., Liao, J. (2016). "Fabrication and compression test of titanium alloy three dimensional lattice structure," *Chinese Journal of Rare Metal* 38(6), 283-291.
- Zhou, J., Feng, X., Zhou, X. (2016). "Experimental research on mechanical properties of larch glulam," *Journal of Central South University of Forestry Technology* 36(8), 125-129.
- Zhu, X., and Luo, J. (2017). "Application of wood esthetics in the development of interior decoration materials," *Furniture Interior Design* (2), 72-74.

Article submitted: February 27, 2018; Peer review completed: May 29, 2018; Revised version received: July 1, 2018; Accepted: July 2, 2018; Published: July 11, 2018.

DOI: 10.15376/biores.13.3.6577-6590